Variable Pore Size, Variable Chemical Functionality, and an Example of Reactivity within Porous Phenylacetylene Silver Salts

Y.-H. Kiang, Geoffrey B. Gardner, Stephen Lee,* Zhengtao Xu, and Emil B. Lobkovsky

Contribution from the Department of Chemistry and Chemical Biology, Baker Laboratory, Cornell University, Ithaca, New York 14853-1301

Received April 7, 1999

Abstract: Investigations on molecular variants of the 3-fold symmetric 1,3,5-tris(4-ethynylbenzonitrile)benzene crystallized with silver triflate revealed a nearly invariant pseudohexagonal porous structure type. Modifications involved the attachment of pendant groups to the central aromatic ring of the parent molecule. Pendant groups include the vinyl group, stilbene, the chiral group myrtanol, and groups with different chemical functionalities such as alcohols, ethers, and esters. Modifications also included the addition of elongated spacer units between the central benzene ring and the peripheral nitrile groups. In these molecules the acetylene bridges of 1,3,5-tris(4-ethynylbenzonitrile)benzene were replaced with diacetylene, ethynylbenzene, and diethynylbenzene type units. Single-crystal refinements for pentoxy-2,4,6-tris(4-ethynylbenzonitrile)benzene·AgOTf and 1,3,5-tris-(4-(4-ethynylbenzonitrile)phenyl)benzene·AgOTf as well as powder data on 12 crystalline phases showed the consistent formation of pseudohexagonal channels, demonstrating that the parent porous architecture is stable both to functional modification of the interior of the channel as well as to enlargement of the pores. Pentoxy-2,4,6-tris(4-ethynylbenzonitrile)benzene·AgOTf refined in the monoclinic space group *Am*. 1,3,5-Tris(4-(4-ethynylbenzonitrile)phenyl)benzene·AgOTf was found to be triclinic with space group $P\bar{1}$. These crystals have pseudohexagonal channels respectively 15 and 25 Å in diameter. Cell constants based on powder data are compatible with channel diameters ranging from 10 to 30 Å. The latter channel diameters are among the largest known for organic porous solids. The introduction of the chiral myrtanol unit led to the preparation of a chiral porous solid. The thermal and chemical stabilities of these phases were investigated. The pseudohexagonal structure proved stable to complete solvent loss from the channel. It was found in the case of a host with alcohol functionality that an acid anhydride guest, trifluoroacetic anhydride, reacted with the host to form an ester with retention of the porous structure type.

Introduction

There has recently been a renewed interest in largely organic systems whose crystalline structures and porous natures are reminiscent of traditional inorganic zeolites.[1−22] A potentially attractive feature of such systems is that by careful selection of the constituent molecules one can potentially modify the inclusion cavities.[23] However, one problem with such an approach is that modification of these organic building blocks often results in global structural changes such as unwanted interpenetrations,[18,24−32] altered network connectivities,[20,33,34] and new metal coordination environments[35−38] which can

* To whom correspondence should be addressed.

(1) MacNicol, D. D.; McKendrick, J. J.; Wilson, D. R. In *Inclusion Compounds*; Atwood, J. L., Davies, J. E., MacNicol, D. D., Eds.; Academic Press: London, 1984; Vol. 2.
(2) Hoskins, B. F.; Robson R. *J. Am. Chem. Soc.* **1990**, *112*, 1546.
(3) Abrahams, B. F.; Hoskins, B. F.; Lin, J.; Robson R. *J. Am. Chem. Soc.* **1991**, *113*, 3045.
(4) Simard, M.; Su, D.; Wuest, J. D. *J. Am. Chem. Soc.* **1991**, *113*, 4696.
(5) Ermer, O.; Lindenberg, L. *Helv. Chim. Acta* **1991**, *74*, 825.
(6) Fujuta, M.; Kwon, Y. J.; Washizu, S.; Ogura, K. *J. Am. Chem. Soc.* **1994**, *116*, 1151.
(7) Abrahams, B. F.; Hoskins, B. F.; Michail, D. M.; Robson, R. *Nature* **1994**, *369*, 727.
(8) Gardner, G. B.; Venkataraman, D.; Moore, J. S.; Lee, S. *Nature* **1995**, *374*, 792.
(9) Venkataraman, D.; Gardner, G. B.; Lee, S.; Moore, J. S. *J. Am. Chem. Soc.* **1995**, *117*, 11600.
(10) Ung, A.; Gizachew, D.; Bishop, R.; Scudder, M.; Dance, I.; Craig, D. *J. Am. Chem. Soc.* **1995**, *117*, 8475.
(11) Endo, K.; Sawaki, T.; Koyanagi, M.; Kobayashi, K.; Masuda, H.; Aoyama, Y. *J. Am. Chem. Soc.* **1995**, *117*, 8341.
(12) Lu, J.; Harrison, W. T. A.; Jacobson, A. J. *Angew. Chem.* **1995**, *107*, 2759; *Angew. Chem., Int. Ed. Engl.* **1995**, *34*, 2557.
(13) Dolbeq, A.; Boubekeur, K.; Batail, P.; Canadell, E.; Aubansenzier, P.; Coulon, C.; Lerstrup, K. *Mater. Chem.* **1995**, *5*, 1707.
(14) Gardner, G. B.; Kiang, Y.-H.; Lee, S.; Asgaonkar, A.; Venkataraman, D. *J. Am. Chem. Soc.* **1996**, *118*, 6946.
(15) Yaghi, O. M.; Li, H.; Groy, T. L. *J. Am. Chem. Soc.* **1996**, *118*, 9096.
(16) Brunet, P.; Simard, M.; Wuest, J. D. *J. Am. Chem. Soc.* **1997**, *119*, 2737.
(17) Yaghi, O. M.; Davis, C. E.; Li, G.; Li, H. *J. Am. Chem. Soc.* **1996**, *119*, 2861.
(18) Hoskins, B. F.; Robson, R.; Slizys, D. A. *Angew. Chem., Int. Ed.* **1997**, *36*, 2336
(19) MacGillivray, L.; Atwood, J. *Nature* **1997**, *389*, 496.
(20) Fujita, M.; Aoyagi, M.; Ogura, K. *Bull. Chem. Soc. Jpn.* **1998**, *71*, 1799.
(21) Batten, S. R.; Robson, R. *Angew. Chem., Int. Ed.* **1998**, *37*, 1461.
(22) Abrahams, B. F.; Jackson, P. A.; Robson, R. *Angew. Chem., Int. Ed.* **1998**, *37*, 2656.
(23) Russel, V. A.; Evans, C. C.; Li, W.; Ward, M. D. *Science (Washington, D.C.)* **1997**, *276*, 575.
(24) Copp, S. B.; Subramanian, S.; Zawortko, M. *J. Am. Chem. Soc.* **1992**, *114*, 8719.
(25) Ermer, O.; Eling, A. *Angew. Chem., Int. Ed. Engl.* **1988**, *27*, 829.
(26) Michaelides, A.; Kiritsis, V.; Skoulika, S.; Aubry, A. *Angew. Chem., Int. Ed. Engl.* **1993**, *32*, 1495.
(27) Reddy, D. S.; Craig, D. C.; Desiraju, G. R. *J. Am. Chem. Soc.* **1996**, *118*, 4090.
(28) Ermer, O. *J. Am. Chem. Soc.* **1988**, *110*, 3747.
(29) Konoshita, Y.; Matsubara, I.; Higuchi, T.; Saito, Y. *Bull. Chem. Soc. Jpn.* **1959**, *32*, 1221.
(30) Ermer, O. *Adv. Mater.* **1991**, *3*, 608.

10.1021/ja991100b CCC: $18.00
Published on Web 08/25/1999

destroy the desired host properties of the solid.[39−42] For example, one of the most studied host−guest systems is that based on Dianin's compound. However, of sixteen derivatives of the parent,[1] only eight exhibit the same inclusion properties as Dianin's compound. In another well-investigated system Bishop and Dance et al. have found a remarkable diol host system for which stringent variants repeatedly adopt a porous morphology. However, even here of thirteen studied derivatives of the host compound, seven form noninclusion solid-state structures.[34,43−48] Furthermore, it is often challenging to predict the substituent effect on the final structure. A good illustration of this is the Bishop and Dance system for which the methyl derivative is porous whereas the hydrogen and ethyl derivatives are not.[34] This difficulty of predicting the final structure highlights the need for parent systems which consistently direct the adoption of a host structure type even in the presence of substantial building block alterations.

One approach to this packing problem is the selection of molecular geometries which naturally not only give rise to porosity but also present sites for modification which are spatially removed from structurally important intermolecular network linkages. This modification at a distance, which perforce requires fairly large organic molecules, potentially allows both expansion of the cavital dimensions as well as the ability to define the interior shape. This is especially true as it is now well established that polytopic ligands[49−56] may be used in the synthesis of extended solids.[57−71] We report here that variants of 1,3,5-tris(4-ethylbenzonitrile)benzene (**1**) persistently crystallize with silver(I) trifluoromethanesulfonate (AgOTf)[8] into structure types based on nearly regular hexagonal channels. Such hexagonal channels are found even in the presence of significant changes to the organic ligands, and thus this preparative methodology can be used to tune both the shape and dimensions of the cavity.

In particular we considered two types of substitution of the parent molecule **1**. In the first set, shown in Figure 1, we placed different substituents on the centered benzene ring of molecule **1** ranging from hydrocarbons to ether, alcohol, and ester linkages. Such alterations were used to test the stability of the porous system to modification of the interior of the hexagonal channels. We also prepared a second set of compounds, also shown in Figure 1, in which the initial acetylene bridging units of molecule **1** are replaced by increasingly long linear rigid units. Such modifications were used to study the stability of the pseudohexagonal architecture to greater cavity dimensions. In both suites of molecules, the crystalline structure of the organic molecule with AgOTf was found to contain nearly regular hexagonal channels. The stability of these hexagonal channels is further proven by an experiment in which a covalent bond forming reaction occurred between an acid anhydride guest, trifluoroacetic anhydride, and an alcohol host molecule **6**·AgOTf without destroying the initial hexagonal pores.

Experimental Section

General Procedure. Unless otherwise indicated, all commercially available reagents were purchased from Aldrich and used without further purification. Analytical grade solvents were obtained from commercial suppliers (Aldrich, Burdick and Jackson, EM Science, Fisher Scientific, and Mallinckrodt).

Powder X-ray diffraction data were recorded on an Enraf-Nonius Gunier Camera at 40 kV, 13 mA for Cu Kα1, $\lambda = 1.5406$ Å, with an internal standard of $RbZn_4Ga_5S_{12}$.[72] Lattice constants were fitted and powder data were indexed by a least-squares method.

Single-crystal X-ray data were collected on a Siemens Smart diffractometer equipped with a CCD area detector using Mo Kα

(31) Sinzger, K.; Hünig, S.; Jopp, M.; Bauer, D.; Bietsch, W.; von Shütz, J. U.; Wolf, H. C.; Kremer, R. K.; Metzenthin, T.; Bau, R.; Kahn, S. I.; Lindbaum, A.; Lengauer, C. L.; Tillmanns, E. *J. Am. Chem. Soc.* **1993**, *115*, 7696.
(32) Hirsch, K. A.; Venkataraman, D.; Wilson, S. R.; Moore, J. S.; Lee, S. *J. Chem. Soc., Chem. Commun.* **1995**, 2199.
(33) Fujita, M.; Kwon, Y.; Sasaki, O.; Yamaguchi, K.; Ogura, K. *J. Am. Chem. Soc.* **1995**, *117*, 7287.
(34) Bishop, R.; Choudhury, S.; Dance, I. *J. Chem. Soc., Perkin Trans. 2* **1982**, 1159.
(35) Kitagawa, S.; Munakata, M.; Tanimura, T. *Inorg. Chem.* **1992**, *31*, 1714.
(36) Kitagawa, S.; Katawa, S.; Kondo, M.; Nozaka, Y.; Munakata, M. *Bull. Chem. Soc. Jpn.* **1993**, *66*, 3387
(37) Carlucci, L.; Ciani, G.; Proserpio, D.; Sironi, A. *Angew. Chem.* **1995**, *107*, 2037; *Angew. Chem., Int. Ed. Engl.* **1995**, *34*, 1895.
(38) Carlucci, L.; Ciani, G.; Proserpio, D.; Sironi, A. *J. Chem. Soc., Chem. Commun.* **1996**, 1393.
(39) Dŭrčanská, E.; Jamnický, M.; Koman, M.; Wnek, I.; Glowiak, T. *Acta. Crystallogr., Sect. C* **1986**, *42*, 1157.
(40) Dŭrčanská, E.; Koman, M.; Jamnický, M. *Acta. Crystallogr., Sect. C* **1991**, *47*, 1193.
(41) Drew, M.; Gray, N.; Cabral, M.; Cabral, J. *Acta. Crystallogr., Sect. C* **1985**, *41*, 1434.
(42) Nassimbeni, L.; Niven, M.; Taylor, M. *Acta. Crystallogr., Sect. B* **1990**, *46*, 354.
(43) Bishop, R.; Craig, D.; Scudder, M. *J. Chem. Soc., Perkin Trans. 2* **1989**, 1473.
(44) Hawkins, S.; Scudder, M.; Craig, D.; Rae, A. D.; Raof, A.; Bishop, R.; Dance, I. *J. Chem. Soc., Perkin Trans. 2* **1990**, 855.
(45) Hawkins, S.; Bishop, R.; Craig, D.; Dance, I.; Rae, A. D.; Scudder, M. *J. Chem. Soc., Perkin Trans. 2* **1993**, 1737.
(46) Bishop, R.; Craig, D.; Dance, I.; Scudder, M.; Marchard, A.; Wang, Y. *J. Chem. Soc., Perkin Trans. 2* **1993**, 937.
(47) Mallick, M.; Bishop, R.; Craig, D.; Dance, I.; Scudder, M. *Aust. J. Chem.* **1991**, *44*, 343.
(48) Ahn, P.; Bishop, R.; Craig, D. C.; Downing, G. A.; Scudder, M. L. *Aust. J. Chem.* **1997**, *50*, 1053.
(49) Konnert, J.; Britton, D. *Inorg. Chem.* **1966**, *5*, 1193.
(50) Hoskins, B. F.; Robson R. *J. Am. Chem. Soc.* **1989**, *111*, 5962.
(51) Abrahams, B. F.; Batten, S. R.; Hamit, H.; Hoskins, B. F.; Robson, R. *J. Chem. Soc., Chem. Commun.* **1996**, 1313.
(52) Venkataraman, D.; Lee, S.; Moore, J. S.; Zhang, P.; Hirsch, K. A.; Gardner, G. B.; Covey, A. C.; Prentice, C. L. *Chem. Mater.* **1996**, *8*, 2030.
(53) Fujita, M.; Ibukuro, F.; Yamaguchi, K.; Ogura, K. *J. Am. Chem. Soc.* **1995**, *117*, 4175.
(54) Yaghi, O. M.; Li, G. *Angew. Chem., Int. Ed. Engl.* **1995**, *34*, 207.
(55) Fujita, M.; Aoyagi, M.; Ibukuro, F.; Ogura, K.; Yamaguchi, K. *J. Am. Chem. Soc.* **1998**, *120*, 611.
(56) Su, D.; Wang, X.; Simard, M.; Wuest, J. D. *Supramol. Chem.* **1995**, *6*, 171.
(57) Carlucci, L.; Ciani, G.; Proserpio, D. M.; Sironi, A. *Inorg. Chem.* **1995**, *34*, 5698.
(58) Carlucci, L.; Ciani, G.; Proserpio, D. M.; Sironi, A. *J. Am. Chem. Soc.* **1995**, *117*, 4562.
(59) Otieno, T.; Rettig, S. J.; Thompson, R. C.; Trotter, J. *Inorg. Chem.* **1993**, *32*, 1607.
(60) Otieno, T.; Rettig, S. J.; Thompson, R. C.; Trotter, J. *J. Can. Chem.* **1989**, *67*, 1964.
(61) Otieno, T.; Rettig, S. J.; Thompson, R. C.; Trotter, J. *J. Can. Chem.* **1990**, *68*, 1901.
(62) MacGillivray, L. R.; Subramanian, S.; Zaworotko, M. J. *J. Chem. Soc., Chem. Commun.* **1994**, *11*, 1325.
(63) Cromer, D. T.; Larson, A. C. *Acta. Crystallogr.* **1972**, *B28*, 1052.
(64) Carlucci, L.; Ciani, G.; Proserpio, D. M.; Sironi, A. *J. Chem. Soc., Chem. Commun.* **1994**, 2755.
(65) Kuroda-Sowa, T.; Horino, T.; Yamamoto, M.; Ohno, Y.; Maekawa, M.; Munakata, M. *Inorg. Chem.* **1997**, *36*, 6382.
(66) Venkataraman, D.; Gardner, G. B.; Covey, A. C.; Lee, S.; Moore, J. S. *Acta Crystallogr.* **1996**, *52*, 2416.
(67) Lopez, S.; Kahraman, M.; Harmata, M.; Keller, S. W. *Inorg. Chem.* **1997**, *36*, 6138.
(68) Lu, J.; Crisci, G.; Niu, T.; Jacobson, A. J. *Inorg. Chem.* **1997**, *36*, 5140.
(69) Hirsch, K. A.; Wilson, S. R.; Moore, J. S. *Chem. Eur. J.* **1997**, *3*, 765.
(70) Blake, A. J.; Champness, N. R.; Khlobystov, A.; Lemenovskii, D. A.; Li, W.-S.; Schroder, M. *J. Chem. Soc., Chem. Commun.* **1997**, 2027.
(71) Abrahams, B. F.; Hardie, M. J.; Hoskins, B. F.; Robson, R.; Sutherland, E. E. *J. Chem. Soc., Chem. Commun.* **1994**, 1049.
(72) Schwer, H.; Keller, E.; Krämer, V. Z. *Z. Kristallogr.* **1993**, *204*, 203.

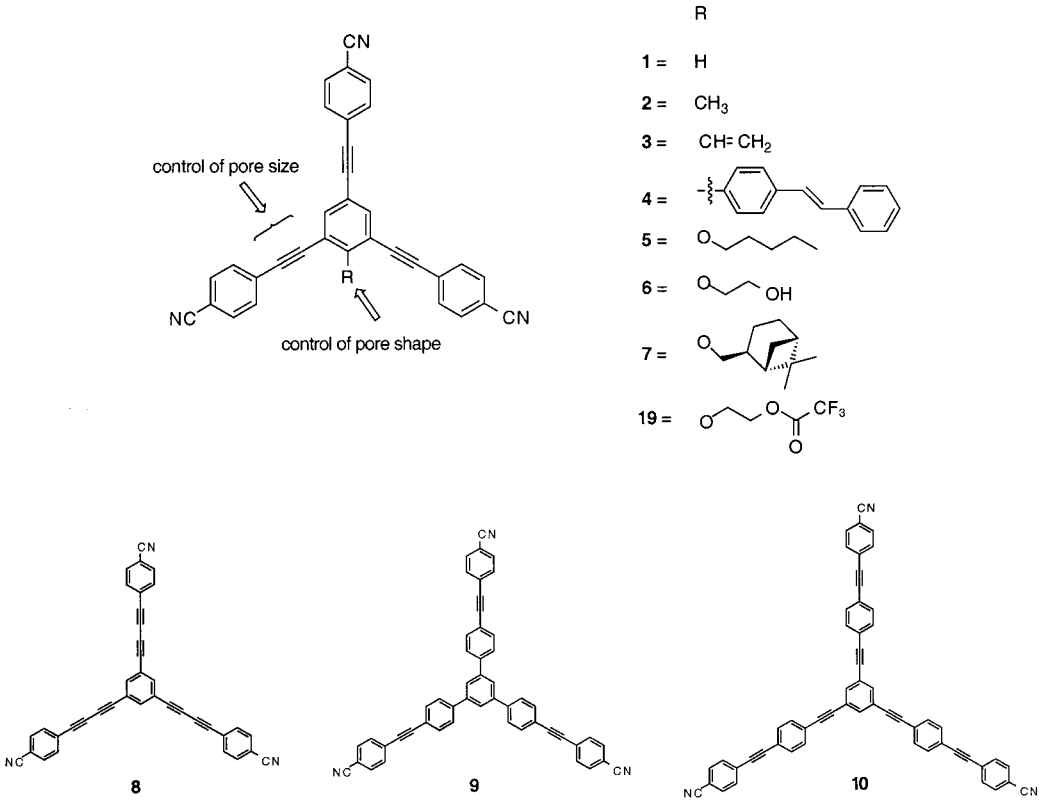

Figure 1. Parent ligand **1** with modifications **2**−**10** and **19**. Modifications **2**−**7** and **19** lead to changes in the interior geometry of the pseudohexagonal channels of their respective silver salts. Modifications **8**−**10** increase the diameters of the pseudohexagonal channels.

radiation. Diffraction data were collected at 293 K. All structure solutions were obtained by a direct method and refined using full-matrix least squares with Shelxl 97. Tables of bond distances, bond angles, and anisotropic thermal factors appear in the Supporting Information.

^{1}H NMR and ^{13}C NMR were performed on a Bruker AC-200, AM-300, or A-360 at 25 °C. Apohosts were prepared on a Perkin-Elmer 7 thermal analyzer.

[2,4,6-Tribromo-4′-(*trans*-2-phenylethenyl)biphenyl (11). A heavy-walled Schlenk flask equipped with a magnetic stirrer was charged with 2,4,6-tribromoiodobenzene (13.0 g, 29.4 mmol), 4-iodostilbene (2.0 g, 6.54 mmol), and powdered copper metal (6.7 g, 0.106 mmol). The flask was evacuated and sealed with a Teflon screw cap under vacuum. Under constant stirring, the temperature of the reaction mixture was raised to 200 °C over a period of 6 h. The solid was then suspended in methylene chloride (100 mL) and filtered through a fritted glass funnel followed by several washings of the residue solid with methylene chloride (3 × 100 mL). The combined filtrate was evaporated to dryness under reduced pressure on a rotary evaporator, and the residue was purified by column chromatography on silica gel (hexanes) to yield **11** as a white solid (2.1 g, 66%): ^{1}H NMR (300 MHz, $CDCl_3$) δ 7.81 (s, 2H), 7.61 (d, J = 7.2 Hz, 2H), 7.38 (t, J = 7.1 Hz, 2H), 7.29 (d, J = 7.2 Hz, 1H), 7.17 (m, 4H); ^{13}C NMR (90 MHz, $CDCl_3$) δ 142.0, 139.5, 137.6, 137.4, 134.5, 129.7, 128.9, 128.3, 128.0, 126.8, 126.6, 125.1, 122.1.

2,4,6-Tribromostyrene (12). A heavy-walled Schlenk flask equipped with a magnetic stirrer was charged with 2,4,6-tribromoiodobenzene (2.0 g, 4.54 mmol), tributyl(vinyl)tin (1.74 g, 5.46 mmol), copper(I) iodide (43 mg, 0.226 mmol), triphenylarsine (0.276 g, 0.902 mmol), bis(dibenzylideneacetone)palladium(0) (0.12 g, 0.209 mmol), and dry tetrahydrofuran (30 mL). The flask was capped with a septum, evacuated, and back-filled with nitrogen three times. The flask was sealed with a Teflon screw cap and stirred at 65 °C for 20 h. The mixture was cooled to room temperature and evaporated to dryness under reduced pressure on a rotary evaporator, and the residue was purified by column chromatography on silica gel (hexanes) to yield **12** as a white crystalline solid (0.64 g, 42%): ^{1}H NMR (300 MHz, $CDCl_3$) δ 7.72 (s, 2H), 6.54 (dd, J = 7.7, 4.5 Hz, 1H), 5.67 (dd, J = 11.5, 1.2 Hz, 1H), 5.62 (dd, J = 17.7, 1.2 Hz, 1H); ^{13}C NMR (75 MHz, $CDCl_3$) δ 137.7, 134.6, 134.4, 123.8, 123.1, 121.0.

Pentoxy-2,4,6-tribromobenzene (13). To a flask equipped with a magnetic stirrer and a reflux condenser were added 2,4,6-tribromophenol (6.0 g, 18.1 mmol), *n*-iodopentane (10.8 g, 54.4 mmol), potassium carbonate (4.0 g, 28.9 mmol), and acetone (40 mL), and the mixture was heated at reflux overnight. After the solution was allowed to cool to room temperature, the mixture was extracted with ether (100 mL) and water (100 mL). The filtrate was washed with 5% sodium hydroxide solution (100 mL) and water (100 mL) and dried over magnesium sulfate. The solvent was removed under reduced pressure on a rotary evaporator to yield **13** as a yellow oil (6.24 g, 86%): ^{1}H NMR (300 MHz, $CDCl_3$) δ 7.64 (s, 2H), 3.97 (t, J = 6.6 Hz, 2H), 1.84 (m, 2H), 1.44 (m, 4H), 0.94 (t, J = 7.1 Hz, 3H); ^{13}C NMR (75 MHz, $CDCl_3$) δ 153.2, 135.0 119.2, 117.1, 73.9, 29.9, 28.2, 22.8, 14.3.

(1*S*,2*S*,5*S*)-Myrtanoxy-2,4,6-triiodobenzene (14). A flask equipped with a magnetic stirrer was charged with sodium (0.4 g, 17.4 mmol) and anhydrous ethanol (50 mL). After the sodium had dissolved, 2,4,6-triiodophenol (8.20 g, 17.4 mmol) was added, and the solution was heated at reflux for 10 min. The solvent was removed in vacuo, and the residual salt was dissolved in 35 mL of THF−DMSO (1:1). A solution of myrtanol tosylate (5.3 g, 17.2 mmol) in anhydrous THF (15 mL) was added via syringe at room temperature and stirred at 60 °C for 3 h. After the solution was allowed to cool to room temperature, the mixture was extracted with 10% K_2CO_3 in water (100 mL) and petroleum ether (100 mL), and the organic layer was dried over sodium sulfate. The solvent was removed under reduced pressure on a rotary evaporator and passed through a plug of silica gel (petroleum ether), and the filtrate was concentrated under reduced pressure to yield **14** as a white solid (5.2 g, 48%): ^{1}H NMR (360 MHz, $CDCl_3$) δ 8.04 (s, 2H), 3.80−3.69 (m, 2H), 1.84 (m, 2H), 2.71−2.60 (m, 1H) 2.27−2.22 (m, 1H) 2.17−2.10 (m, 1H), 1.94−1.67 (m, 1H) 1.52−1.33 (m, 2H), 1.26 (s, 3H), 0.93 (s, 3H); ^{13}C NMR (75 MHz, $CDCl_3$) δ 158.1, 147.3, 92.3, 89.1, 76.7, 42.6, 41.1, 39.4, 35.9, 27.0, 24.4, 24.2, 20.6, 18.1.

2,4,6-Tris(trimethylsilylethynyl)toluene (15). A heavy-walled Schlenk tube equipped with a magnetic stirrer was charged with 2,4,6-tribromotoluene (2.0 g, 6.08 mmol), copper(I) iodide (0.25 g, 1.32

mmol), bis(triphenylphosphine)palladium(II) chloride (0.25 g, 0.356 mmol), and triethylamine (50 mL). The flask was capped with a septum, evacuated, and back-filled with nitrogen. Trimethylsilylacetylene (3.58 g, 36.5 mmol) was added to the flask under nitrogen via syringe. The flask was sealed with a Teflon screw cap and stirred at 80−90 °C for 12 h. The reaction mixture was then allowed to cool to room temperature and filtered through a fritted glass funnel. The filtrate was evaporated to dryness under reduced pressure on a rotary evaporator on silica gel (3:1 hexanes−chloroform) to yield **15** as a waxy solid (1.79 g, 77%): ^{1}H NMR (300 MHz, $CDCl_3$) δ 7.49 (s, 2H), 2.52 (s, 3H), 0.25 (s, 18H), 0.22 (s, 9H); ^{13}C NMR (90 MHz, $CDCl_3$) δ 143.5, 135.6, 123.9, 120.8, 99.4, 94.8, 88.2, 19.7, 0.1.

2,4,6-Tris(trimethylsilylethynyl)-4′-(*trans*-2-phenylethenyl)biphenyl (16). A heavy-walled Schlenk flask was charged with **11** (1.96 g, 3.98 mmol), copper(I) iodide (0.163 g, 0.858 mmol), triphenylphosphine (0.652 g, 2.49 mmol), bis(triphenylphosphine)palladium(II) chloride (0.163 g, 0.232 mmol), and triethylamine (50 mL). The flask was capped with a septum, evacuated, and back-filled with nitrogen. Trimethylsilylacetylene (2.37 g, 24.2 mmol) was added to the flask *via* syringe. The flask was sealed with a Teflon cap and stirred at 80−90 °C for 12 h. The reaction mixture was then allowed to cool to room temperature and filtered through a glass funnel. The filtrate was evaporated under reduced pressure on a rotary evaporator and the residue purified by column chromatography on silica gel (3:1 cyclohexane−chloroform) to yield **16** as a yellow solid (1.34 g, 62%): ^{1}H NMR (300 MHz, $CDCl_3$) δ 7.62 (s, 2H), 7.58−7.48 (m, 6H), 7.38 (t, J = 7.2 Hz, 2H), 7.28 (m, 1H), 7.17 (s, 2H), 0.26 (s, 9H), 0.07 (s, 18H); ^{13}C NMR (75 MHz, $CDCl_3$) δ 146.5, 137.4, 136.0, 130.7, 128.9, 127.8, 126.7, 125.4, 123.4, 122.4, 103.3, 99.2, 95.9, 0.18, −0.14.

Pentoxy-2,4,6-tris(trimethylsilylethynyl)benzene (17). A heavy-walled Schlenk flask equipped with a magnetic stirrer was charged with **13** (1.05 g, 2.62 mmol), copper(I) iodide (0.11 g, 0.589 mmol), triphenylphosphine (0.44 g, 1.53 mmol), bis(triphenylphosphine)-palladium(II) chloride (0.11 g, 0.157 mmol), and triethylamine (50 mL). The flask was capped with a septum, evacuated, and back-filled with nitrogen. Trimethylsilylacetylene (1.54 g, 15.7 mmol) was added to the flask *via* syringe. The flask was sealed with a Teflon cap and stirred at 80−90 °C for 12 h. The reaction mixture was then allowed to cool to room temperature and filtered through a glass funnel. The filtrate was evaporated under reduced pressure on a rotary evaporator and the residue purified by column chromatography on silica gel (85:15 hexanes−chloroform) to yield **17** as a yellow oil (0.64 g, 54%): ^{1}H NMR (300 MHz, $CDCl_3$) δ 7.64 (s, 2H), 3.97 (t, J = 6.6 Hz, 2H), 1.84 (m, 2H), 1.44 (m, 4H), 0.94 (t, J = 7.1 Hz, 3H); ^{13}C NMR (75 MHz, $CDCl_3$) δ 153.2, 135.0, 119.2, 117.1, 73.9, 29.9, 28.2, 22.8, 14.3.

(2,4,6-Tris(trimethylsilylethynyl)phenoxy)ethanol (18). A heavy-walled Schlenk flask equipped with a magnetic stirrer was charged with (2,4,6-tribromophenoxy)ethanol (3.00 g, 8.00 mmol), copper(I) iodide (0.168 g, 0.882 mmol), triphenylphosphine (0.64 g, 2.57 mmol), bis-(triphenylphosphine)palladium(II) chloride (0.168 g, 0.239 mmol), and triethylamine (50 mL). The flask was capped with a septum, evacuated, and back-filled with nitrogen. Trimethylsilylacetylene (3.92 g, 40.0 mmol) was added to the flask *via* syringe. The flask was sealed with a Teflon cap and stirred at 80−90 °C for 12 h. The reaction mixture was then allowed to cool to room temperature and filtered through a glass funnel. The filtrate was evaporated under reduced pressure on a rotary evaporator and the residue purified by column chromatography on silica gel (65:35 hexanes−chloroform) to yield **18** as a clear oil (3.08 g, 91%): ^{1}H NMR (360 MHz, $CDCl_3$) δ 7.50 (s, 2H), 4.39 (t, J = 4.2 Hz, 2H), 3.82 (t, J = 4.4 Hz, 2H), 0.23 (s, 18H), 0.22 (s, 9H); ^{13}C NMR (75 MHz, $CDCl_3$) δ 161.2, 139.2, 119.1, 117.7, 102.8, 100.8, 100.0, 19.1, 16.2, 1.26.

2,4,6-Tris(4-ethynylbenzonitrile)toluene (2). A Schlenk flask equipped with a magnetic stirrer was charged with **15** (0.30 g, 0.789 mmol) and tetrahydrofuran (50 mL). The mixture was capped with a septum, evacuated, back-filled with nitrogen, and cooled to 5 °C in an ice bath. A 1.0 M solution of tetrabutylammonium fluoride in 9:1 tetrahydrofuran−water (2.7 mL, 2.7 mmol) was added rapidly *via* syringe. After 5 min the solution was concentrated to near dryness under reduced pressure on a rotary evaporator, and the residue was eluted through a plug of silica gel with a 9:1 hexanes−chloroform solution. The filtrate was evaporated to dryness under reduced pressure on a rotary evaporator and transferred to a heavy-walled Schlenk flask. To this flask were added 4-bromobenzonitrile (0.862 g, 4.74 mmol), copper(I) iodide (33 mg, 0.174 mmol), triphenylphosphine (0.160 g, 0.611 mmol), bis(triphenylphosphine)palladium(II) chloride (33 mg, 0.047 mmol), and triethylamine (50 mL). The flask was capped with a septum, evacuated, back-filled with nitrogen, sealed with a Teflon cap, and stirred at 80−90 °C for 12 h. The reaction mixture was then allowed to cool to room temperature and filtered through a glass funnel. The filtrate was evaporated under reduced pressure on a rotary evaporator and the residue purified by column chromatography on silica gel (CH_2Cl_2) to yield **2** as a beige solid (0.2 g, 50%): ^{1}H NMR (300 MHz, $CDCl_3$) δ 7.72 (s, 2H), 7.70 (d, J = 7.9 Hz, 2H), 7.66 (q, J = 6.7 Hz, 8H), 7.61 (d, J = 8.6 Hz, 2H), 2.72 (s, 3H); ^{13}C NMR (75 MHz, $CDCl_3$) δ 143.5, 135.6, 132.3, 132.2, 127.7, 123.8, 120.6, 118.4, 112.3, 112.2, 92.9, 91.7, 91.0, 88.8, 19.6; MS (EI, 70 eV) *m*/*z* 486 (38), 467 (100), 466 (17); IR (KBr, cm^{-1}) 2924, 2228, 2214, 1602, 1497, 1173, 1103, 836; HRMS (EI, 70 eV) calcd 467.1422, found 467.1415.

2,4,6-Tris(4-ethynylbenzonitrile)styrene (3). A heavy-walled Schlenk flask equipped with a magnetic stirrer was charged with **12** (50 mg, 0.15 mmol) 4-ethynylbenzonitrile[73] (65 mg, 0.51 mmol), copper(I) iodide (1.1 mg, 5.8 μmol), triphenylphosphine (3.9 mg, 15 μmol), bis-(triphenylphosphine)palladium(II) chloride (33 mg, 0.047 mmol), and triethylamine (3 mL). The flask was capped with a septum, evacuated, back-filled with nitrogen, sealed with a Teflon cap, and stirred at 70 °C for 20 h. The reaction mixture was then allowed to cool to room temperature and filtered through a glass funnel. The filtrate was evaporated under reduced pressure on a rotary evaporator and the residue purified by column chromatography on silica gel (CH_2Cl_2) to yield **3** as a yellow solid (38 mg, 53%): ^{1}H NMR (300 MHz, $CDCl_3$) δ 7.76 (s, 2H), 7.69−7.60 (m, 12H), 7.19 (dd, J = 17.7, 5.6 Hz, 1H), 6.43 (dd, J = 17.7, 1.2 Hz, 1H), 5.82 (dd, J = 5.6, 1.2 Hz, 1H); ^{13}C NMR (75 MHz, $CDCl_3$) δ 140.9, 136.5, 132.8, 132.1, 132.0, 127.4, 122.2, 121.8, 121.4, 118.2, 112.2, 112.1, 92.9, 91.3, 89.5; MS (EI, 70 eV) *m*/*z* 481 (12), 480 (43), 479 (100), 478 (20), 477 (16); IR (KBr, cm^{-1}) 3057, 2924, 2228, 2214, 1602, 1457, 1173, 1103, 836; HRMS (EI, 70 eV) calcd 479.1422, found 479.1412.

2,4,6-Tris(4-ethynylbenzonitrile)-4′-(*trans*)-2-phenylethenyl)biphenyl (4). A Schlenk flask equipped with a magnetic stirrer was charged with **16** (0.40 g, 0.735 mmol) and tetrahydrofuran (50 mL). The mixture was capped with a septum, evacuated, back-filled with nitrogen, and cooled to 5 °C in an ice bath. A 1.0 M solution of tetrabutylammonium fluoride in 9:1 tetrahydrofuran−water (2.2 mL, 2.2 mmol) was added rapidly *via* syringe. After 5 min the solution was concentrated to near dryness under reduced pressure on a rotary evaporator, and the residue was eluted through a plug of silica gel with a 7:3 hexanes−chloroform solution. The filtrate was evaporated to dryness under reduced pressure on a rotary evaporator and transferred to a heavy-walled Schlenk flask. To this flask were added 4-bromobenzonitrile (0.442, 2.43 mmol), copper(I) iodide (20 mg, 0.105 mmol), triphenylphosphine (0.104 g, 0.397 mmol), bis(triphenylphosphine)-palladium(II) chloride (26 mg, 0.037 mmol), and triethylamine (50 mL). The flask was capped with a septum, evacuated, back-filled with nitrogen, sealed with a Teflon cap, and stirred at 80−90 °C for 12 h. The reaction mixture was then allowed to cool to room temperature and filtered through a glass funnel. The filtrate was evaporated under reduced pressure on a rotary evaporator and the residue purified by column chromatography on silica gel (chloroform) to yield **4** as a yellow solid (0.32 g, 67%): ^{1}H NMR (360 MHz, $CDCl_3$) δ 7.84 (s, 2H), 7.67 (q, J = 9.0 Hz, 6H), 7.60 (d, J = 8.2 Hz, 4H), 7.56 (d, J = 6.7 Hz, 4H), 7.41 (t, J = 7.1 Hz, 2H), 7.31 (m, 5H), 7.23 (s, 2H); ^{13}C NMR (90 MHz, $CDCl_3$) δ 146.7, 137.5, 136.9, 135.8, 132.2, 132.0, 131.9, 130.5, 129.6, 128.8, 128.1, 128.0, 127.4, 126.6, 123.1, 122.0, 112.1, 111.9, 92.1, 91.3, 89.4; MS (EI, 70 eV) *m*/*z* 633 (16), 632 (56), 631 (100), 630 (19), 554 (13), 529 (21); IR (KBr, cm^{-1}) 2221, 2214, 1602, 1497, 836, 688; HRMS (EI, 70 eV) calcd 631.2048, found 631.2075.

(73) Takahashi, S.; Kuroyama, Y.; Sonogashi, K.; Hagihara, N. *Synthesis* **1980**, *8*, 627.

(74) Lavastre, O.; Cabioch, S.; Dixneuf, P. H. *Tetrahedron* **1997**, *53*, 7595.

Pentoxy-2,4,6-tris(4-ethynylbenzonitrile)benzene (5). A Schlenk flask equipped with a magnetic stirrer was charged with **17** (0.45 g, 1.00 mmol) and tetrahydrofuran (50 mL). The mixture was capped with a septum, evacuated, back-filled with nitrogen, and cooled to 5 °C in an ice bath. A 1.0 M solution of tetrabutylammonium fluoride in 9:1 tetrahydrofuran−water (3.2 mL, 3.2 mmol) was added rapidly *via* syringe. After 5 min the solution was concentrated to near dryness under reduced pressure on a rotary evaporator, and the residue was eluted through a plug of silica gel with a 7:3 hexanes−chloroform solution. The filtrate was evaporated to dryness under reduced pressure on a rotary evaporator and transferred to a heavy-walled Schlenk flask. To this flask were added 4-bromobenzonitrile (1.09, 5.99 mmol), copper(I) iodide (42 mg, 0.221 mmol), triphenylphosphine (0.210 g, 0.802 mmol), bis(triphenylphosphine)palladium(II) chloride (42 mg, 0.060 mmol), and triethylamine (50 mL). The flask was capped with a septum, evacuated, back-filled with nitrogen, sealed with a Teflon cap, and stirred at 80−90 °C for 12 h. The reaction mixture was then allowed to cool to room temperature and filtered through a glass funnel. The filtrate was evaporated under reduced pressure on a rotary evaporator and the residue purified by column chromatography on silica gel (chloroform) to yield **5** as a white solid (0.34 g, 63%): ^{1}H NMR (360 MHz, $CDCl_3$) δ 7.70 (s, 2H), 7.68 (d, J = 8.6 Hz, 4H), 7.66 (d, J = 8.5 Hz, 2H), 7.61 (d, J = 8.6 Hz, 4H), 7.59 (d, J = 8.7 Hz, 2H), 4.38 (t, J = 6.3 Hz, 2H), 1.84 (m, 3H), 1.36 (m, 4H), 0.87 (t, J = 7.3 Hz, 3H); ^{13}C NMR (75 MHz, $CDCl_3$) δ 161.8, 137.4, 132.2, 132.1, 132.0, 127.7, 118.4, 117.9, 117.4, 112.2, 112.0, 92.9, 91.4, 88.8, 88.5, 75.2, 30.4, 28.5, 22.7, 14.2; MS (EI, 70 eV) *m*/*z* 540 (10), 470 (42), 469 (100), 440 (10); IR (KBr, cm^{-1}) 2931, 2227, 1602, 1499, 1442, 1236, 1175, 1113, 837; HRMS (EI, 70 eV) calcd 539.1998, found 539.1990.

(2,4,6-Tris(4-ethynylbenzonitrile)phenoxy)ethanol (6). A Schlenk flask equipped with a magnetic stirrer was charged with **18** (1.00 g, 2.35 mmol) and tetrahydrofuran (50 mL). The mixture was capped with a septum, evacuated, back-filled with nitrogen, and cooled to 5 °C in an ice bath. A 1.0 M solution of tetrabutylammonium fluoride in 9:1 tetrahydrofuran−water (8.3 mL, 8.3 mmol) was added rapidly *via* syringe. After 5 min the solution was concentrated to near dryness under reduced pressure on a rotary evaporator, and the residue was eluted through a plug of silica gel with chloroform. The filtrate was evaporated to dryness under reduced pressure on a rotary evaporator and transferred to a heavy-walled Schlenk flask. To this flask were added 4-bromobenzonitrile (1.71, 9.40 mmol), copper(I) iodide (49 mg, 0.257 mmol), triphenylphosphine (0.200 g, 0.763 mmol), bis(triphenylphosphine)-palladium(II) chloride (49 mg, 0.070 mmol), and triethylamine (50 mL). The flask was capped with a septum, evacuated, back-filled with nitrogen, sealed with a Teflon cap, and stirred at 80−90 °C for 12 h. The reaction mixture was then allowed to cool to room temperature and filtered through a glass funnel. The filtrate was evaporated under reduced pressure on a rotary evaporator and the residue purified by column chromatography on silica gel (chloroform) to yield **5** as a white solid (0.30 g, 25%): ^{1}H NMR (360 MHz, $CDCl_3$) δ 7.73 (s, 2H), 7.71−7.61 (m, 12H), 4.50 (t, J = 4.2 Hz, 2H), 3.99 (t, J = 4.2 Hz, 2H); ^{1}H NMR (300 MHz, acetone-d_6) δ 7.89−7.77 (m, 14H), 4.55 (t, J = 4.8 Hz, 2H), 4.02 (t, J = 4.8 Hz, 2H); ^{13}C NMR (90 MHz, $CDCl_3$) δ 160.9, 137.4, 132.4, 132.3, 132.2, 127.5, 127.2, 118.8, 118.5, 118.4, 117.7, 112.5, 112.2, 93.6, 91.1, 88.9, 88.1, 76.4, 62.1; IR (KBr, cm^{-1}) 3428, 3066, 2228, 1603, 1501, 1460, 1443, 1406, 1242, 1117, 1106, 1071, 883, 837; HRMS (EI, 70 eV) calcd 513.1477, found 513.1460.

(1*S*,2*S*,5*S*)-Myrtanoxy-2,4,6-tris(4-ethynylbenzonitrile)benzene (7). A Schlenk flask equipped with a magnetic stirrer was charged with **14** (1.00 g, 2.35 mmol), 4-ethynylbenzonitrile (1.3 g, 10.20 mmol), copper(I) iodide (30 mg, 0.15 mmol), triphenylphosphine (170 mg, 0.65 mmol), bis(dibenzylideneacetone)palladium(0) (90 mg, 0.17 mmol), and triethylamine (30 mL). The flask was capped with a septum, evacuated, back-filled with nitrogen, sealed with a Teflon cap, and stirred at 50 °C for 12 h. The reaction mixture was then allowed to cool to room temperature and filtered through a glass funnel. The filtrate was evaporated under reduced pressure on a rotary evaporator and the residue purified by column chromatography on silica gel (chloroform) to yield **7** as a yellow solid (1.2 g, 53%): $[\alpha]^{23}_D = -7.22°$ (c = 0.024 in $CHCl_3$); ^{1}H NMR (360 MHz, $CDCl_3$) δ 7.71 (s, 2H), 7.69−7.69 (m, 12H), 4.21−4.12 (m, 2H), 2.59 (m, 1H), 2.19 (t, J = 5.2 Hz, 1H), 2.04−1.98 (m, 1H), 1.90−1.84 (m, 1H), 1.82−1.68 (m, 2H), 1.16 (s, 3H), 0.87 (s, 3H); ^{13}C NMR (75 MHz, $CDCl_3$) δ 161.9, 137.5, 127.2, 118.5, 118.4, 117.9, 117.3, 112.2, 112.0, 93.0, 91.5, 88.8, 88.6, 78.5, 42.8, 41.1, 39.5, 36.3, 26.9, 24.3, 23.9, 20.5, 18.4; IR (KBr, cm^{-1}) 2923, 2806, 2227, 2213, 1603, 1499, 1440, 1405, 1374, 1234, 1175, 1116, 1103, 989, 836, 756, 552.

1,3,5-Tris(4-butadiynylbenzonitrile)benzene (8). A Schlenk flask equipped with a magnetic stirrer was charged with 4-bromoethynylbenzonitrile (0.77 g, 3.73 mmol) and ethanol (40 mL). To this rapidly stirring mixture were dropwise added a solution of NH_2OH·HCl (62 mg, 0.90 mmol), *n*-butylamine (1.68 g, 23.0 mmol), copper(I) chloride (1.0 g, 0.01 mmol), and 1,3,5-triethynylbenzene (186 mg, 1.24 mmol) in ethanol (5 mL) at room temperature. This flask was then evacuated, back-filled with nitrogen, capped with a Teflon cap, and stirred at room temperature. After 2 h, the precipitate was filtered and chromatographed on silica gel (CH_2Cl_2) to yield **8** as a yellow solid (128 mg, 20%): ^{1}H NMR (300 MHz, $CDCl_3$) δ 7.67 (s, 3H), 7.64 (m, 12H); ^{13}C NMR (90 MHz, $CDCl_3$) δ 136.9, 133.2, 132.3, 126.4, 123.1, 118.3, 113.1, 81.0, 80.8, 75.5; IR (KBr, cm^{-1}) 3057, 2924, 2228, 2214, 1602, 1457, 1173, 1103, 836; HRMS (EI, 70 eV) calcd 525.1266, found 525.1260.

1,3,5-Tris(4-(4-ethynylbenzonitrile)phenyl)benzene (9). A heavy-walled Schlenk flask equipped with a magnetic stirrer was charged with 1,3,5-tris(4-bromophenyl)benzene (700 mg, 1.3 mmol) 4-ethynylbenzonitrile (10.6 g, 4.7 mmol), copper(I) iodide (2.5 mg, 0.15 mmol), triphenylphosphine (34 mg, 0.13 mmol), bis(dibenzylideneacetone)-palladium(0) (14 mg, 26 μmol), and triethylamine (30 mL). The flask was capped with a septum, evacuated, back-filled with nitrogen, sealed with a Teflon cap, and stirred at 70 °C for 16 h. The reaction mixture was then allowed to cool to room temperature and filtered through a glass funnel. The filtrate was evaporated under reduced pressure on a rotary evaporator and the residue purified by column chromatography on silica gel (CH_2Cl_2) to yield **9** as a yellow solid (0.33 g, 37%): ^{1}H NMR (300 MHz, $CDCl_3$) δ 7.85 (s, 3H), 7.76−7.74 (m, 24H); ^{13}C NMR (90 MHz, $CDCl_3$) δ 141.7, 141.3, 132.1, 127.4, 125.4, 121.7, 118.5, 111.6, 93.5; IR (KBr, cm^{-1}) 3039, 2224, 2217, 1599, 1515, 1017, 832; HRMS (EI, 70 eV) calcd 681.2205, found 681.2177.

1,3,5-Tris(4-(4-ethynylbenzonitrile)benzoethylnyl)benzene (10). A heavy-walled Schlenk flask equipped with a magnetic stirrer was charged with 1-trimethylsilylethynyl-4-((4-cyanophenyl)-ethynyl)benzene (500 mg, 1.7 mmol), potassium carbonate (0.12 g, 0.80 mmol), and a methanol−dichloromethane (1:3) solution (20 mL) and then the mixture was stirred under nitrogen for 3 h. This mixture was transferred to another heavy-walled Schlenk flask equipped with a magnetic stirrer which was then charged with 1,3,5-tribromobenzene (153 mg, 0.48 mmol), copper(I) iodide (1.0 mg, 5.3 μmol), triphenylphosphine (12.6 mg, 48 μmol), bis(dibenzylideneacetone)palladium(0) (5.2 mg, 9.7 μmol), and triethylamine (10 mL). The flask was capped with a septum, evacuated, back-filled with nitrogen, sealed with a Teflon cap, and stirred at 70 °C for 16 h. The reaction mixture was then allowed to cool to room temperature and filtered through a glass funnel. The filtrate was evaporated under reduced pressure on a rotary evaporator and the residue purified by column chromatography on silica gel (CH_2Cl_2) to yield **10** as a yellow solid (148 mg, 41%): ^{1}H NMR (300 MHz, $CDCl_3$) δ 7.66 (s, 3H), 7.62−7.56 (m, 12H), 7.53 (s, 12H); ^{13}C NMR (90 MHz, $CDCl_3$) δ 134.2, 132.0, 131.7, 131.6, 127.8, 123.8, 123.3, 122.4, 118.3, 111.7, 93.1, 90.2, 89.9, 89.6; IR (KBr, cm^{-1}) 2226, 2217, 1658, 1600, 1579, 1103, 835; HRMS (EI, 70 eV) calcd 753.2205, found 753.2184.

Preparation of Microcrystalline Powders 1·, 2·, 3·, 4·, 5·, 7·, 8·, 9·, and 10·AgOTf. The organic ligand (40 mg, 0.1 mmol) was dissolved in benzene (10 mL) and added to a solution of silver(I) trifluoromethanesulfonate (25 mg, 0.1 mmol) in benzene (10 mL) in a vial sealed with a Teflon-lined screw cap. The vial was heated in a programmable furnace equipped with a Eurotherm temperature controller from 1 to 100 °C, held at 100 °C for 60 min, and then cooled to room temperature at 0.02 °C/min. The resultant crystalline powder was composed of particles typically 25 μm × 10 μm × 10 μm as determined by optical microscopy.

Preparation of Microcrystalline Powders 6· and 19·AgOTf. The organic ligand (40 mg, 0.1 mmol) was dissolved in benzene (10 mL) and acetone (1 mL), and then the solution was added to a solution of silver(I) trifluoromethanesulfonate (25 mg, 0.1 mmol) in benzene (10

mL). The vial was left undisturbed and exposed to the atmosphere to allow escape of solvent. Crystalline precipitate typically formed after 24 h.

Preparation of X-ray-Quality Single Crystals of 5·AgOTf. A solution of silver(I) trifluoromethanesulfonate (0.9 mg, 25 μmol) in benzene (1.5 mL) was added to a solution of **5** (2 mg, 3.5 μmol) in benzene (1.5 mL) in a clean vial. A white precipitate formed immediately, which was then dissolved by adding acetonitrile (0.3 mL). Slow evaporation of the solvents yielded six single crystals suitable for X-ray data collection after seven days.

Preparation of X-ray-Quality Single Crystals of 9·AgOTf. A solution of silver(I) trifluoromethanesulfonate (0.05 mg, 0.2 μmol) in benzene (1.5 mL) was added to a solution of **9** (0.13 mg, 0.2 μmol) in benzene (1.5 mL) in a clean vial. Slow evaporation of the solvent yielded three single crystals suitable for X-ray data collection after 10 days.

Preparation and Vapor Exchange of Apohosts 4·, 5·, and 7·AgOTf. The crystals grown in benzene were first filtered until the supporting filter paper was slightly damp. The sample was then immediately placed in a thermogravimetric analyzer (TGA) and heated from room temperature to 200 °C at 10 °C/min under nitrogen to void the solid of initially included solvent (**4**·AgOTf was heated only to 120 °C). The apohost was then suspended above benzene, taking care to maintain spatial separation between host and guest, and then sealed in a vial. The vial was heated to 40 °C for 20 h. Powder patterns of these materials were obtained from special glass capillary tubes.

Solid-State Esterfication of 6·AgOTf. 6·AgOTf crystals grown in benzene were gravity filtered until the supporting filter paper was slightly damp. A Schlenk tube was prepared with trifluoroacetic anhydride at its bottom and a loose glass wool plug in its neck. The sample was immediately transferred onto this glass wool. The tube was then exposed to vacuum for 10 s before being sealed. After 1 h the tube was pumped down to an ultimate pressure of 15 mTorr to remove excess anhydride. Following this same procedure, the sample was further allowed to react, this time though in a Schlenk tube charged with benzyl alcohol. In this latter procedure the tube was initially exposed to vacuum for 15 min rather than 10 s. The final sample was analyzed by XRD, IR, and ^{1}H NMR: ^{1}H NMR (300 MHz, acetone-d_6) δ 7.89−7.77 (m, 14H), 4.93 (s, 4H); IR (KBr, cm^{-1}) 3444, 2232, 1788, 1604, 1501, 1409, 1222, 1165, 1037.

Trifluoroacetic ((2,4,6-Tris(4-ethynylbenzonitrile)phenoxy))ethyl Ester (19). 6 (5.8 mg, 0.01 mmol) in CH_2Cl_2 (3 mL) was added to trifluoroacetic anhydride (1.05 g, 5 mmol). This solution was stirred at room temperature for 10 min and then evacuated to dryness to yield **19** as a white solid (100% by thin layer chromatography): ^{1}H NMR (300 MHz, $CDCl_3$) δ 7.73 (s, 2H), 7.70−7.60 (m, 12H), 4.76 (dd, J = 3.3, 2.2 Hz, 2H), 4.69 (dd, J = 3.3, 2.2 Hz, 2H); ^{1}H NMR (300 MHz, acetone-d_6) δ 7.89−7.75 (m, 14H), 4.90 (s, 4H); IR (KBr, cm^{-1}) 3431, 2228, 1788, 1603, 1501, 1402, 1221, 1155, 837; MS (FAB) m/z (M^+) 609 (14).

Results and Discussion

Functionalized Structures 2−7· and 19·AgOTf. In Scheme 1 we show the general synthetic route to molecules **1**−**7**.[75] Preparation of powder crystalline samples of **1**−**7**· and **19**· AgOTf and single crystals of **5**·AgOTf and **9**·AgOTf is further described in the previous section. We begin our discussion of these systems with the crystal structure of **5**·AgOTf, illustrated in Figure 2b. A summary of parameters for the X-ray data collection and subsequent refinement is given in Table 1. We compare this structure to the previously reported[14] structure of **1**·AgOTf illustrated in Figure 2a. In both structures each silver ion is coordinated to three nitrogen atoms in a trigonal planar environment while each organic molecule is in turn coordinated to three silver ions again in a trigonal planar manner. Silver−nitrogen distances range from 2.26 to 2.12 Å for **1**·AgOTf and from 2.24 to 2.21 Å for **5**·AgOTf. The triflate ions remain near the silver cation. In the compound **1**·AgOTf, oxygen atoms of one of the triflate anions form relatively weak bonds with a Ag−O bond distance of 2.4 Å while the other triflate anion forms no oxygen−silver bonds. In **5**·AgOTf, due to crystalline disorder, it proved impossible to locate the oxygen atoms of the triflate anion. However, the more heavy sulfur ion could be located. One sulfur atom lies 3.32 Å from a Ag ion while the other sulfur atoms are 5.20 Å away from silver ions. By

(75) For **7**, the starting material was the triiodide (1*S*,2*S*,5*S*)-Myrtanoxy-2,4,6-triiodobenzene, and for **3** and **7**, the trihalides were directly reacted with the 4-ethynylbenzonitrile to make the desired final products. See the Experimental Section for specific reactions.

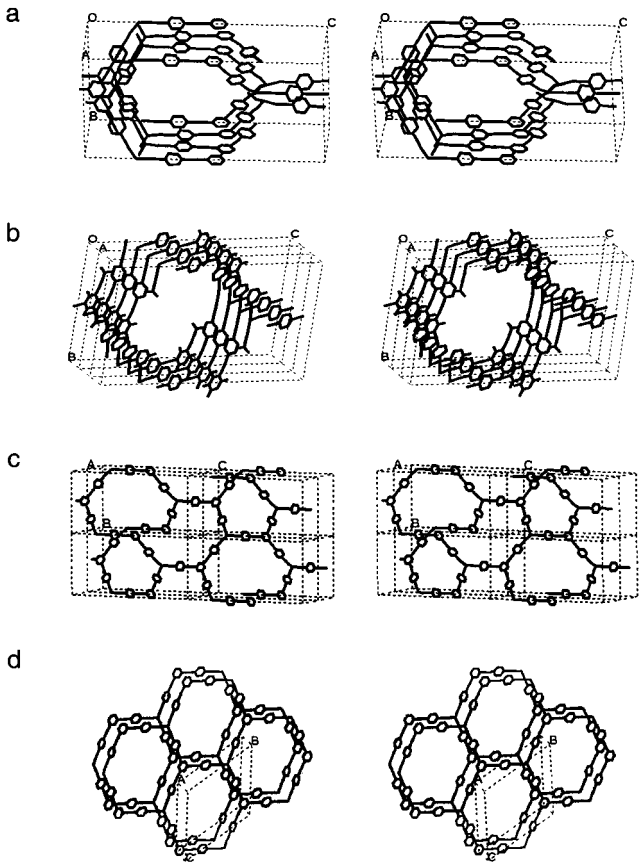

Figure 2. View down the *a* axis of (a) **1**·AgOTf and (b) **5**·AgOTf showing the pseudohexagonal channels. Solvent molecules and triflate ions have been removed for clarity. (c) A single net of **1**·AgOTf oriented to show its three-dimensional character. (d) Two eclipsed nets of **5**· AgOTf.

Scheme 1

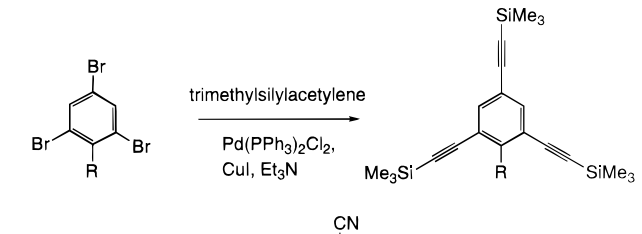

Table 1. Crystal Data and Structure Refinement for **5**·AgOTf

formula	$C_{39}H_{25}Ag_1F_3N_3O_4S_1$
formula weight	748.55
T, K	173(2)
wavelength, Å	0.71073
crystal system	monoclinic
space group	*Am*
a, Å	3.7528(8)
b, Å	22.259(5)
c, Å	32.295(7)
$\alpha = \gamma$, deg	90
β, deg	92.65(3)
V, Å^3	2694.8(10)
Z	2
ρ_{calcd}, g/cm^3	0.923
absorption coefficient, mm^{-1}	0.445
θ range for data collection, deg	1.83−20.30
limiting indices	$-4 \le h \le 4$, $-9 \le k \le 24$, $-20 \le l \le 33$
no. of data/restraints/parameters	2575/11/152
no. of reflections collected/unique reflections	2873/2757
absorption correction	SADABS
goodness-of-fit on F^2	1.765
$R1$[a]	0.117 ($I > 2\sigma(I)$)
$wR2$[a]	0.2887 ($I > 2\sigma(I)$)

[a] $R1 = \sum||F_c| - |F_o||/\sum|F_o|$, $wR2 = [\sum[w(F_o^2 - F_c^2)]^2/\sum[w(F_o^2)^2]]^{1/2}$.

comparison, in **1**·AgOTf·benzene Ag−S distances are 3.55 and 5.00 Å. The similarity of the shorter of the two sulfur−silver distances suggests that one of the oxygen atoms on some triflate ions is coordinated to a silver atom.

The probable proximate cause for the crystalline disorder in **5**·AgOTf is that the molecule **5** itself has lower point group symmetry than the D_{3h} symmetry of molecule **1**. In particular the pentoxy group is covalently attached to only one of the three possible sites on the central benzene ring. In the solved single-crystal structure model this pentoxy group is found to be disordered with an equal distribution of three possible orientations of this molecule. Due to this disorder only the oxygen atom of the pentoxy group could be located as may be seen by inspection of Figure 2a.

The overall crystal structures shown in Figure 2a,b are related to one another. Passing through the center of the unit cell in both figures are slightly irregular hexagonal channels. In both structures, there are two such hexagonal channels per unit cell running along the *a* axis. Despite the similar coordination environments of the two structures and the similarity of their pseudohexagonal channels, the structures represented in Figure 2a,b are quite different. This is most clearly seen in Figure 2c,d. In these two illustrations we have emphasized the overall topology of the network connectivity in **1**·AgOTf and **5**·AgOTf. In Figure 2d one sees that the trigonal planar coordination leads to planar honeycomb sheets which stack one on top of each other in a nearly eclipsing fashion along the *a* axis. By contrast, the crystal structure of **1**·AgOTf is three-dimensional with half the trigonal planes oriented one way and half another way.

Both network types illustrated in Figure 2c,d correspond to well-known inorganic crystal structure types. In Figure 3 we illustrate the known network formed by the boron atoms in AlB_2 and by the silicon atoms in $ThSi_2$. It may be seen that, just as in **5**·AgOTf, the boron atoms of AlB_2 form into planar honeycomb sheets which lie eclipsed to each other. By contrast the silicon atoms of $ThSi_2$ form a three-dimensional array like the one found in **1**·AgOTf. Following standard practice where network types are named after original members of the structural families, it seems appropriate to term the structures of **1**·AgOTf and **5**·AgOTf as, respectively, the $ThSi_2$ and AlB_2 types.

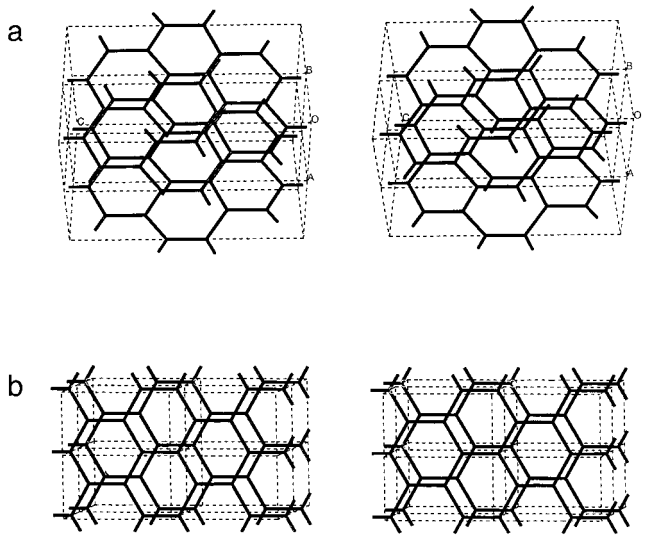

Figure 3. (a) Three-dimensional silicon network in $ThSi_2$ oriented to show its pseudohexagonal channels. (b) Two-dimensional boron net in AlB_2.

In both crystal structures shown in Figure 2, the hexagonal channels do not have perfect hexagonal symmetry. This can be seen by examining the ratio of the *c* and *b* axes. In the case of a perfect hexagonal channel placed into an orthorhombic cell $c/b = \sqrt{3} = 1.71$.[76] In **1**·AgOTf this ratio is elongated while in **5**·AgOTf it is shortened to *c*/*b* values of, respectively, 2.029 and 1.491. The structural cause for these deviations may be understood by examining Figure 2a,b. In Figure 2a one of the three arms of molecule **1** lies directly along the *c* cell axis while the other two arms are rotated in such a way as to shorten the *b* axis from its maximal possible value, hence shifting the *c*/*b* ratio to larger values. Similarly in Figure 2b the honeycomb sheets are rotated out of the *bc* plane. The axis of rotation can be taken to be the *a* axis itself. Hence, the *b* axis length corresponds to the ideal hexagonal cell axis length while the *c* axis is shortened with respect to the ideal value. In **5**·AgOTf the *c*/*b* ratio therefore is smaller than the ideal *c*/*b* ratio.

Of particular importance are the *c* axis length of the $ThSi_2$ type structure and the *b* axis length of the AlB_2 structure. This is so these lengths can be directly compared to distances calculated from known bond distances. Assuming standard tabulated bond lengths[77] and a Ag to N distance of 2.21 Å, one finds a distance of 13.02 Å between the center of the molecules **1**−**7** and the adjacent silver ions. For the $ThSi_2$ structure, we find that the *c* axis is invariant and should be 3 times this distance or 39.06 Å while for AlB_2 the *b* axis is also invariant and should be $\sqrt{3}$ times this distance or 22.55 Å. These theoretical values compare well with the single-crystal lattice parameters of, respectively, 38.75 and 22.26 Å for **1**·AgOTf and **5**·AgOTf. Such comparisons will be used in this paper for systems for which there are only powder data and for which one wishes to distinguish between the AlB_2 and $ThSi_2$ structural alternatives.

We now turn to the other substituted versions of **1**·AgOTf·benzene, to **2**−**7**· and **19**·AgOTf. As Figure 1 shows this includes a range of substituents ranging from both saturated and unsaturated hydrocarbon moieties to ether, alcohol, and ester groups. Of particular interest is **7**, a chiral substituent, which

(76) In this paper the *a* cell axis is pointed consistently in the direction of the channels. Were the structure truly hexagonal, the *a* axis would then be (unconventionally) the unique axis.

(77) March, J. *Advanced Organic Chemistry*, 4th ed.; Wiley: New York, 1992; p 21.

will perforce lead to a chiral crystal structure. As we were unable to prepare crystals suitable for single-crystal X-ray diffraction, we consider instead X-ray powder data. We find in these systems that the powder data give strong insight into the actual crystal structures. An illustration of these powder data is given in Figure 4 for **1**·AgOTf·toluene, **1**·AgOTf·benzyl alcohol, **5**·AgOTf, and **6**·AgOTf. Also shown in Figure 4 is the calculated powder pattern based on the single-crystal data for **1**·AgOTf·benzene. As may be seen, not only do the various powder patterns all look rather similar to one another, there is also excellent agreement between the observed powder patterns and those calculated from the single-crystal models.

The refined cell constants for **2**−**7**· and **19**·AgOTf are given in Table 2. In Table 2, we report only values for *c*, *b*, and α. This is due to the high Debye−Waller factors in these systems. Due to these high values the decay in intensity as a function of θ is significant, as may be seen in Figure 4. Recalling that for **5**·AgOTf the *a* cell axis is only 3.75 Å, this decay means that while we generally have a reasonable number of reflections (10−20 reflections) to index the larger *c* and *b* axes, there are only two to three reflections useful for determining *a*, β, and γ. Hence, only values for the former lattice parameters are reliable.

It may be seen that the cell axes in Table 2 separate into three somewhat distinct families. In the first family *b* and *c* axes are, respectively, 19−20 and 38−39 Å while for the second and third family *b* is 22.2−22.7 Å. The distinction between the second and third families is in their *c* axes. In the former compounds *c* axes are 33−34 Å while for the latter systems they are 35−36 Å. Thus, while the division between the type one compounds and the others is quite sharp, that between types two and three is somewhat diffuse.

Given the agreement of both the intensities of the observed reflections and the near equivalence of the cell parameters, it is reasonable to expect that all type one compounds are isotypic with the $ThSi_2$ structure reported for **1**·AgOTf·benzene. Similarly, agreement in both reflection intensities and cell parameters suggests that all type two systems are isotypic with the AlB_2 structure reported for **5**·AgOTf. For type three compounds it would appear the structure is also of AlB_2 type, but where the rotation of the honeycomb sheets out of the *bc* plane is reduced with respect to those found for type two.

One curious point is the strong similarity between the powder patterns of the AlB_2 and $ThSi_2$ structures. For example, there is a marked similarity between the $ThSi_2$ pattern shown in Figure 4d and the AlB_2 patterns shown in Figure 4a−c. The source of this similarity may be traced to the similarities in their actual crystal structures. In particular, the data observed in the various powder patterns are 0*kl* reflections. The 0*kl* data set corresponds in real space to the projected electronic density onto the *bc* plane. As may be seen in Figure 2a,b, it is exactly under this projection that the two crystal types most resemble one another. The observed powder pattern can be taken to be the characteristic pattern for pseudohexagonal channels.

It may also be observed that in one respect the AlB_2 and $ThSi_2$ structures differ from one another. Both are distortions of the ideal hexagonal cell axes. Hence, reflections which are degenerate in θ value for a hexagonal cell split into two distinct powder pattern peaks. As noted above, the distortion is an elongation of *c*/*b* for $ThSi_2$ but a diminution for AlB_2. However, as both this elongation and this diminution are roughly equal displacements from the ideal value, the pairs of reflections appear roughly equally spaced but in reversed order in the two different structural families. For example, the pair of reflections

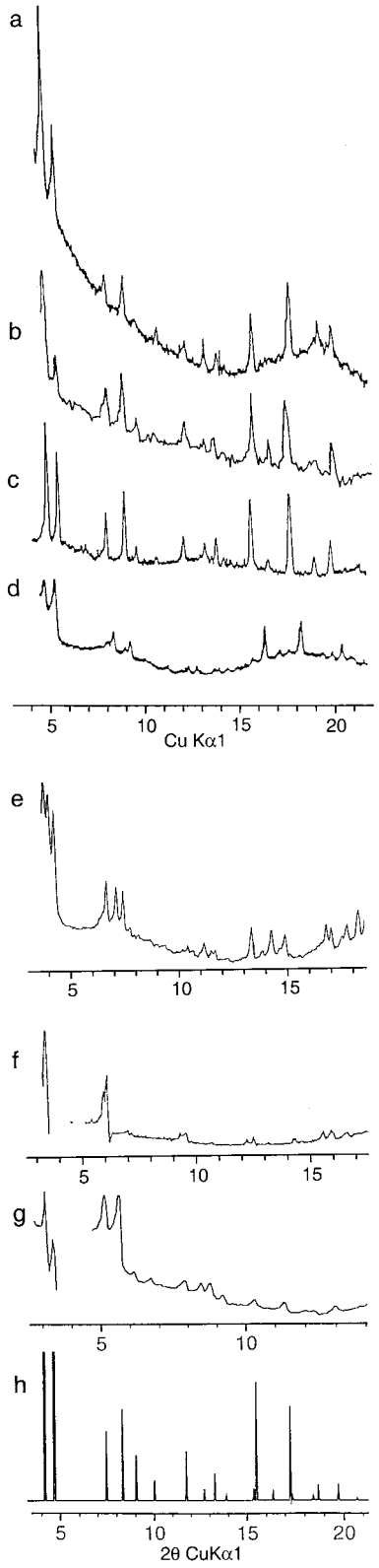

Figure 4. X-ray powder patterns for (a) **1**·AgOTf·benzyl alcohol, (b) **6**·AgOTf·benzene, (c) **5**·AgOTf·benzene, (d) **1**·AgOTf·toluene, (e) **8**·AgOTf·benzene, (f) **9**·AgOTf·benzene, and (g) **10**·AgOTf·benzene and (h) the calculated powder pattern for the 0*kl* reflections of **1**·AgOTf·benzene based on the single-crystal model.

observed at $2\theta = 5°$ in Figure 4 correspond to the 002 and 011 reflections. In the $ThSi_2$ system the 002 reflection is at the lower 2θ value while for the AlB_2 type it is the higher 2θ reflection.

One final point of interest is that one can prepare **1**·AgOTf in both the $ThSi_2$ and AlB_2 structure types. If crystals of **1**·

Table 2. Cell Constants for Phenylacetylene·AgOTf Crystals[a]

compound	*b* (Å)	*c* (Å)	β (deg)	*c*/*b*	structure type	ref
1·AgOTf[b]·benzene	19.110(7)	38.856(15)	90	2.03	$ThSi_2$	14
1·AgOTf·toluene	19.29(2)	39.91(15)	90	2.07	$ThSi_2$	14
1·AgOTf·*m*-xylene	19.58(3)	38.50(5)	90	1.97	$ThSi_2$	14
7·AgOTf·apohost	20.08(2)	37.9(4)	90	1.89		*h*
1·AgOTf·benzyl alcohol	22.43(1)	33.98(2)	90	1.51	AlB_2	14
1·AgOTf[c]·benzene	22.385(2)	33.828(7)	90	1.51	AlB_2	*h*
1·AgOTf·phenol	22.48(2)	34.08(6)	90	1.52	AlB_2	14
2·AgOTf·benzene	22.58(3)	33.42(5)	90	1.48	AlB_2	*h*
3·AgOTf·benzene	22.70(2)	33.37(3)	90	1.47	AlB_2	*h*
5·AgOTf·benzene	22.64(2)	33.43(2)	90	1.47	AlB_2	*h*
5·AgOTf[b]·benzene	22.259(5)	32.295(7)	90	1.45	AlB_2	*h*
6·AgOTf·benzene	22.63(1)	33.23(3)	90	1.46	AlB_2	*h*
7·AgOTf·benzene	22.23(2)	33.82(6)	90	1.52	AlB_2	*h*
19·AgOTf·benzene	22.57(2)	33.58(3)	90	1.49	AlB_2	*h*
19·AgOTf[d]·benzene	22.37(1)	33.91(3)	90	1.51	AlB_2	*h*
19·AgOTf[e]·benzene	22.47(2)	33.95(3)	90	1.51	AlB_2	*h*
1·AgOTf·apohost	22.77(2)	36.39(4)	90	1.60	AlB_2	*h*
4·AgOTf·benzene	22.17(6)	35.22(8)	90	1.58	AlB_2	*h*
5·AgOTf·apohost	22.98(8)	35.42(5)	90	1.54	AlB_2	*h*
8·AgOTf[f]·benzene	24.128(5)	46.441(1)	85.75(2)	1.92		*h*
8·AgOTf[f]·benzene	26.94(5)	41.53(8)	86.87(2)	1.54		*h*
9·AgOTf·benzene	29.106(3)	48.515(7)	90	1.67	AlB_2	*h*
9·AgOTf[g]·benzene	30.327(6)	46.214(7)	90.0(3)	1.52	AlB_2	*h*
10·AgOTf·benzene	34.103(4)	52.751(6)	90	1.55	AlB_2	*h*

[a] Unless otherwise specified, cell constants are from powder data. [b] Single-crystal data. [c] From the solid-state exchange of benzene for benzyl alcohol by placing **1**·AgOTf·benzyl alcohol in liquid benzene. [d] From the solid-state reaction of crystalline **6**·AgOTf·benzene with trifluoroacetic anhydride vapor. [e] From the solid-state reaction of crystalline **6**·AgOTf·benzene with trifluoroacetic anhydride vapor, followed by introduction of benzyl alcohol vapor. [f] Two different *A*-centered pseudorectangular cells corresponding to the same oblique Bravais lattice ($b = 25.362(4)$ Å, $c = 24.128(5)$ Å, $\alpha = 114.07(2)°$). [g] Pseudorectangular supercell of the reported *P*1 Bravais lattice (from single-crystal data). [h] This work.

Scheme 2

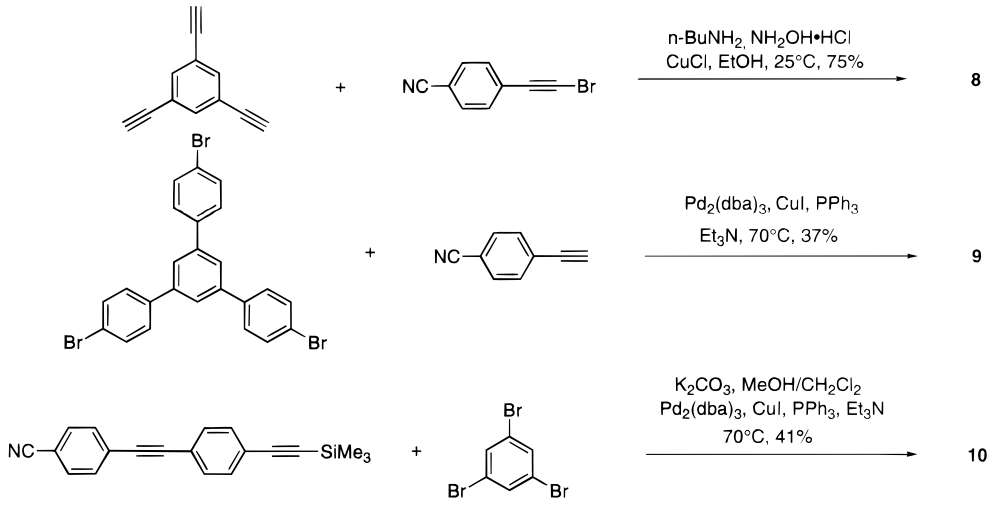

$AgOTf-ThSi_2$ type are placed at room temperature in a benzyl alcohol solution, the crystal cell parameters evolve into the AlB_2 type. Further, if these then altered benzyl alcohol crystals are now placed at room temperature back into benzene solution, the unit cell parameters remain in the honeycomb type. However, ^1H NMR studies show that there is a quantitative replacement of the benzyl alcohol molecules by benzene. Thus, one can prepare **1**·AgOTf·benzene in two different near hexagonal channel structure types. The observed unit cells are given in the first and sixth lines of Table 2. As the cell constants differ by 3−5 Å, it is clear that we have prepared two different forms of the same compound. These results indicate that Ag−nitrile bonds both break and re-form at room temperature in the presence of solvent. It is interesting that optical microscope pictures of crystals of **1**·AgOTf show no change in crystalline morphology, other than a loss of crystal transparency.[14]

Structures with Enlarged Channel Diameters, 8−10·AgOTf. The above data demonstrate the stability of the hexagonal channel structure subject to modifications which change the functional groups in the interior of these channels. We have also studied a series of molecules in which the original 3-fold symmetry of the molecule **1** has been maintained but where the distance between the centered benzene ring and the peripheral nitrile groups has increased from 13.02 to 19.96 Å. The molecules prepared include **8**−**10**. The overall synthetic route to these compounds is shown in Scheme 2. In each case we could prepare microcrystalline samples of the organic molecule together with silver triflate. For **9** it proved possible to find a crystal suitable for a single-crystal X-ray data collection. Parameters relevant to the single-crystal data collection and structure refinement are given in Table 3.

As in the earlier discussed crystal structures, the trigonal organic molecule **9** is coordinated to three silver ions through linear nitrile to silver bonds. There are two crystallographically

Table 3. Crystal Data and Structure Refinement for **9**·AgOTf·4.5benzene

formula	$C_{79}H_{54}Ag_1F_3N_3O_3S_1$
formula weight	1290.18
T, K	173(2)
wavelength, Å	0.71073
crystal system	triclinic
space group	$P\bar{1}$
a, Å	14.3765(11)
b, Å	27.628(2)
c, Å	27.648(2)
α, deg	66.549(2)
β, deg	84.674(3)
γ, deg	79.620(3)
V, Å^3	9906.9(13)
Z	4
ρ_{calcd}, g/cm^3	0.865
absorption coefficient, mm^{-1}	0.264
θ range for data collection, deg	0.8−17.23
limiting indices	$-11 \le h \le 11$, $-23 \le k \le 16$, $-23 \le l \le 23$
no. of data/restraints/parameters	11525/12/724
no. of reflections collected/unique reflections	21609/11525
absorption correction	SADABS
goodness-of-fit on F^2	1.212
$R1^a$	0.157 ($I > 2\sigma(I)$)
$wR2^a$	0.4005 ($I > 2\sigma(I)$)

[a] $R1 = \sum||F_c| - |F_o||/\sum|F_o|$, $wR2 = [\sum[w(F_o^2 - F_c^2)]^2/\sum[w(F_o^2)^2]]^{1/2}$.

inequivalent silver atoms in the structure. Both silver atoms are bonded to three nitrogen atoms; in both cases Ag−N bond distances range from 2.08 to 2.23 Å with Ag−N coordination environments that are nearly trigonal planar. The N−Ag−N bond angles for Ag1 are 105.1°, 113.8°, and 129.1° while for Ag2 they are 112.9°, 120.1°, and 124.8°. The net sum of each set of three angles are 348° for Ag1 and 358° for Ag2. These net sums approach the 360° angles expected for perfectly planar coordination. Also as in the earlier structures the silver ions form a single weak bond to an oxygen atom of a triflate anion. For Ag1 this bond is 2.39 Å long while for Ag2 it is 2.46 Å long.

An illustration of the crystal structure is given in Figure 5. As may be seen we are able to locate the first layer of solvent atoms which are directly adjacent to the rigid phenylacetylene host. More interior to the channel, benzene molecules proved too solvent-like to locate by diffraction methods.

As may be inferred from Figure 5b the overall topology of this crystal is of the AlB_2 type. As in the previous AlB_2 structures the planar honeycomb sheets do not lie exactly in the *bc* planes but instead are rotated out of this plane using the *b* axis as the axis of rotation. For this crystal the *c*/*b* ratio is 1.52, similar to those for the other previously discussed AlB_2 structures. There is however one notable difference between the AlB_2 type structures reported for **5**·AgOTf and **9**·AgOTf. While both these two structures are comprised of stacks of tilted honeycomb sheets, in **5**·AgOTf the silver atoms of one layer lie nearly directly above the silver atoms of the adjacent layer; by contrast in **9**·AgOTf the silver atoms lie half the time above silver atoms and half the time above the central benzene ring of molecule **9**. One therefore needs four layers to form a translational repeat unit for **9**·AgOTf but only a single layer for **5**·AgOTf. This is reflected in the *a* axis lengths for the two crystals of, respectively, 14.38 and 3.75 Å.

We may use the solved crystal structure of **9**·AgOTf to assess the prediction of structure type from cell constants. As before, using literature reference values for organic bond distances and a Ag−N bond distance of 2.21 Å, we find for **9**·AgOTf a 17.3 Å distance between the Ag atom and the center of molecule **9**'s central benzene ring. For an AlB_2 structure the *b* axis length would be roughly 30.0 Å ($\sqrt{3} \times 17.3$) while for the $ThSi_2$ structure we would expect a *c* axis length of 51.9 Å (3×17.3). The actual cell axes are $b = 30.3$ Å and $c = 46.2$ Å. The cell constants clearly suggest that **9**·AgOTf forms in the AlB_2 structure type. Furthermore, the *c*/*b* ratio of 1.52 suggests a tilt angle of the honeycomb layers very similar to the tilt angle found for **5**·AgOTf. An examination of the full single-crystal structure shows that both surmises are correct. However, we were not able to deduce the different stacking sequences actually observed in **9**·AgOTf.

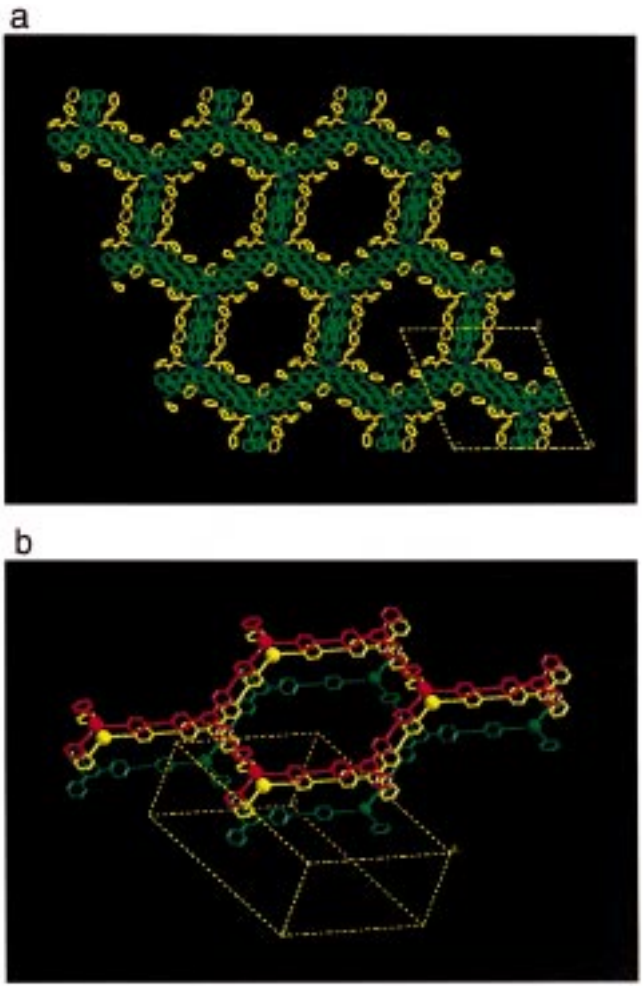

Figure 5. Crystal structure of **9**·AgOTf. (a) Molecule **9** is shown in green, silver in blue, and triflate ions and solvent molecules in yellow. Channel diameters are roughly 25 Å. (b) A view down the *a* axis showing the nearly eclipsed hexagonal layers. The layer on top is red, the middle layer yellow, and the bottom layer green. Silver ions are represented as small spheres.

We now turn to powder samples of **8**−**10**. Their powder patterns are shown in Figure 4. In each case the resultant powder pattern can be indexed to a cell similar in shape to those found for **1**−**7**. The refined cell constants are reported in Table 2. Of the three powder patterns the one for **10**·AgOTf is most similar to the previous powder patterns. Indeed, as Figure 4 shows, except for the scale change in the *θ* angles caused by the larger size of molecule **10**, the similarity between this powder pattern and the ones for **1**−**7**·AgOTf is striking. The cell axis lengths for **10**·AgOTf confirm this similarity. If we use standard carbon−carbon and carbon−nitrogen bond distances[77] and silver−nitrogen bond distances of 2.21 Å, we can calculate a Ag to centered benzene ring distance of 19.9 Å. In the AlB_2

structure type this corresponds to a *b* axis length of 34.4 Å compared to the observed distance of 34.1 Å. The *c*/*b* ratio is 1.55, well within the range of *c*/*b* of 1.47−1.59 found for the other AlB_2 structures. We therefore have good evidence suggesting that **10**·AgOTf forms in the AlB_2 structure type. Channel dimensions have however increased from 10−15 Å for **1**·AgOTf to 25−30 Å for **10**·AgOTf.

For **9**·AgOTf we find two unit cells, one from the powder sample and the other from a single-crystal data set where the crystal was grown from slow evaporation from benzene. The cell parameters are considerably different from one another. In the single-crystal sample, the *b* axis is 1.2 Å longer than that found by the powder pattern while the *c* axis is 2.3 Å shorter than that of the powder pattern. These differences are significantly larger than those typically expected between powder and single-crystal X-ray data. As in our earlier example where **1**·AgOTf·benzene formed in two different structures depending on the route of synthetic growth, it is quite plausible that the differences in solvent and crystal growth conditions change the exact unit cell dimensions while leaving the fundamental powder patterns quite similar.

Among all the powder patterns shown in Figure 4, the powder patterns for **8**· and **9**·AgOTf are the most different. For **9**·AgOTf the different appearance in the powder profile can be attributed to a difference in the *c*/*b* ratio. The observed *c*/*b* ratio is 1.67. This is very near the ideal hexagonal *c*/*b* ratio of 1.71, and therefore the resolution of the densitometer trace of our Gunier film data; many nearly equivalent reflections overlap.

The powder pattern for **8**·AgOTf is the most different from the other reported powder patterns. Whereas in the other powder patterns reflections appear in doublets, reflections for **8**·AgOTf are in triplets. This can be understood in the following way. In a two-dimensional hexagonal cell the three reflections 10, 01, and −11 have exactly equal *d* spacing. In rectangular distortions of a two-dimensional hexagonal cell 10 and 01 can have exactly equal *d* spacing, but −11 has a different *d* spacing. Hence, a rectangular cell leads to a doubling of the original hexagonal reflections. If we further lower the symmetry to an oblique one, 10, 01, and −11 each have different *d* spacings. We therefore tried to index the **8**·AgOTf pattern to such an oblique cell. This proves possible with concomitant good standard deviations in the cell parameters. Two equivalent cells are presented in Table 2. By the previously described method of estimating cell constants for an AlB_2 structure, we find a putative *b* axis of 27 Å while for the $ThSi_2$ structure we find a potential *c* axis of 46.7 Å. In Table 2 we see that in one oblique cell the *b* axis is 26.95 Å and in another oblique cell the *c* axis is 46.4 Å. It is therefore difficult to ascribe to which structure type the **8**·AgOTf corresponds. Nevertheless, the high agreement between d_{calcd} and d_{obsd}, as well as the overall powder pattern intensities, suggests that some sort of pseudohexagonal channels are present in this structure.

Chemical Reactions between Host and Guest. The previous results show that channels of 10−30 Å are present in compounds such as **1**·AgOTf·benzene through **10**·AgOTf·benzene. We now turn to a few illustrative examples of the chemical transformations possible in this general family of compounds. We consider two types of transformations. The first is that of preparing an apohost, i.e., a material in which all the solvent has been removed. As described in the Experimental Section, if we take **5**·AgOTf·benzene or **7**·AgOTf·benzene and quickly heat the samples to 200 °C, we can show by ^{1}H NMR that all the solvent has been removed. The X-ray diffraction data for these systems are given in the Supporting Information. The similarity between these data and the other powder pattern data reported in this paper suggests that their crystal structures are still of the same overall family. As may be seen in Table 2, apohost **5**·AgOTf and apohost **7**·AgOTf have *b* cell axes of 22−23 Å and *c* axes of 35−36 Å. The fairly close agreement of the *b* axes with the *b* axes of **1**−**7**·AgOTf·benzene suggests, just as in those crystals and just as in the single-crystal structure of **5**·AgOTf·benzene, that hexagonal sheets have formed which lie in a plane which includes the *b* axis. The *c* axis is however roughly 2−3 Å longer than what is found for **5**·AgOTf·benzene. This suggests that the structures in these systems are of the AlB_2 type but with a smaller rotation of the honeycomb sheets out of the *bc* plane than that found in the single-crystal structure of **5**·AgOTf·benzene. For one of the unit cells, that of **7**, cell parameters are closer to those of the $ThSi_2$ type.

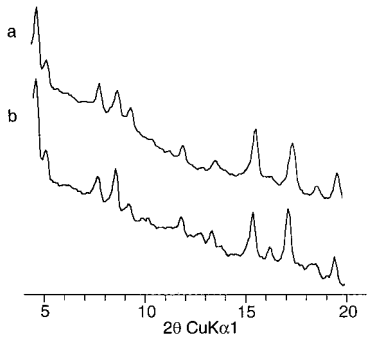

Figure 6. X-ray powder patterns for **6**·AgOTf·benzene (a) before and (b) after exposure to trifluoroacetic anhydride and benzyl alcohol vapor.

We and others have shown that such apohosts can reincorporate a number of guests.[11,78−80] Rather than just repeat earlier experiments, we investigated more stringent conditions on the porosity of the channel structures.[81] We chose to study the reactivity of the channel structure itself. In particular **6**·AgOTf contains an alcohol unit inside the channel. We therefore combined a sample of **6**·AgOTf with a strong electrophile, trifluoroacetic anhydride. While the reaction in solution between an alcohol and an acid anhydride is straightforward and leads to the ester **19**, we need to demonstrate that such a reaction can also take place in the solid state in good yield and with retention of the initial crystal structure.

The design of our experiment is as follows. We first placed a sample of crystalline **6**·AgOTf in the vapor of trifluoroacetic anhydride (bp 39.5−40 °C). After some time we quenched the reactions with benzyl alcohol vapor to remove excess trifluoroacetic anhydride. X-ray powder patterns were taken before reaction, before addition of the benzyl alcohol vapor, and after addition of the benzyl alcohol vapor. The cell constants after each of these steps are shown in Table 2. As may be seen there is little evolution of cell parameters, indicating little change in the overall crystal structure. In Figure 6 we show the actual powder patterns before and after reaction. Again, little change in the diffraction pattern can be seen.

Solid-state IR studies reveal however clear changes. The original crystalline sample shows no bands between 2100 and 1650 cm^{-1}. After addition of the anhydride but before the

(78) Kondo, M.; Okubo, T.; Asami, A.; Noro, S.; Yoshitomi, T.; Kitagawa, S.; Ishii, T.; Matsuzaka, H.; Seki, K. *Angew. Chem., Int. Ed.* **1999**, *38*, 140.

(79) Li, H.; Davis, C. E.; Groy, T. L.; Kelly, D. G.; Yaghi, O. M. *J. Am. Chem. Soc.* **1998**, *120*, 2186.

(80) Li, H.; Eddaoudi, M.; Groy, T. L.; Yaghi, O. M. *J. Am. Chem. Soc.* **1998**, *120*, 8571.

(81) Chui, S.; Lo, S.; Charmant, J.; Orpen, A. G.; Williams, I. D. *Science (Washington, D.C.)* **1999**, *283*, 1148.

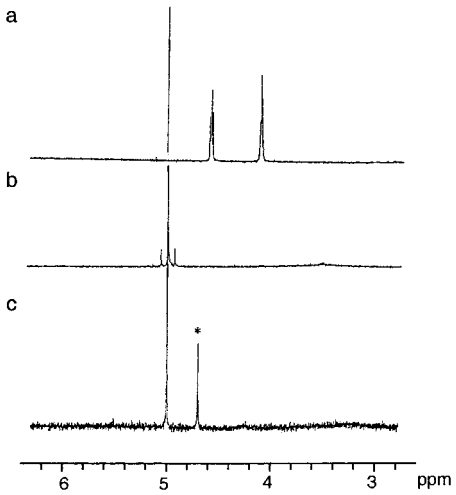

Figure 7. Portion of the 300 MHz ^{1}H NMR spectra of **6**·AgOTf·benzene in acetone-d_6 (a) before exposure to trifluoroacetic anhydride vapor, (b) after exposure to trifluoroacetic anhydride vapor, and (c) after exposure to trifluoroacetic anhydride and benzyl alcohol vapor. Resonances correspond to the methylene protons of the pendant group. In (c) the resonance marked with an asterisk is due to the benzyl alcohol molecule.

addition of the benzyl alcohol, a new peak appears at 1788 cm^{-1}. Such a peak is compatible with the ester **19**. To verify this, we prepared the ester **19** by regular solution methods. The carbonyl peak for this sample was also at 1788 cm^{-1}, in good agreement with our solid-state results.

Further confirmation of the solid-state reaction was found by a solution ^{1}H NMR study. Here again, we took solid-state samples before reaction, after the addition of the anhydride but before addition of benzyl alcohol, and after addition of benzyl alcohol. We then dissolved these solid-state samples in acetone-d_6. The NMR data show that addition of the trifluoroacetic anhydride results in the near quantitative conversion of **6** into a single new compound. The ^{1}H NMR pattern of this latter compound is in excellent agreement with that of molecule **19** prepared by solution reaction methods. The NMR shifts are quite marked for the ethylene region near the reacting alcohol moiety in molecule **6**. We show these data in Figure 7. As a final check that the reaction has indeed taken place, we took molecule **19** and crystallized it with AgOTf. The cell parameters for this compound are reported in Table 2 and are in agreement with the cell parameters of the reacted solid.

We conclude that it is possible to chemically modify the **6**·AgOTf system with a covalent bond to an introduced guest molecule without destroying the overall crystalline topology. Furthermore, the solid-state transformation can be made by introduction of a vapor at room temperature into the solid crystal. These results suggest that the porous crystalline framework is itself intact throughout these transformations.

Conclusion

We have examined 20 crystals in this paper. All of the 20 compounds have similar powder patterns, indicating a common crystalline motif. The three solved single-crystal structures clearly demonstrate that this motif is pseudohexagonal channels which are regularly packed and parallel to one another. The channel structure type exhibits a somewhat unexpected stability. It is stable to modification of the chemical functional groups, to alteration of the size of the channel, to removal of all guest molecules within the channel, and to a covalent bond forming reaction between guest and host. Modifications allowable include the inclusion of ether, alcohol, unsaturated hydrocarbons, and esters. With inclusion of chiral guests, chiral porous hosts could be prepared with diameters ranging from 10 to 30 Å.

We may compare this family of structures to the very important inorganic porous solid MCM-41. In this latter system one is able to prepare rather stable hexagonal channel crystal structures with variable pore sizes ranging up to 100 Å[82] in which the channel walls are entirely composed of strong covalent bonds. The chemical stability of the MCM-41 structure is far superior to the stability of the structures reported in this paper. However, the MCM-41 structure is nearly amorphous at atomic length scales. In this paper we have seen that if we sacrifice the strength of covalent bonds and replace them with coordination bonds, we can prepare porous solids of some chemical stability in a well-crystallized form which allows structural resolution at atomic distances. A clear goal for the future is the preparation of covalently bonded structures which retain the structural resolution of the compounds reported in this paper but also the chemical stability of materials such as MCM-41.

Acknowledgment. This work was supported by the National Science Foundation (Grant DMR-9812351). We thank Professor D. Venkataraman for the synthetic procedure of **9**.

Supporting Information Available: Tables of crystal refinement data, bond distances, bond angles, anisotropic thermal factors for **5**· and **9**·AgOTf, and powder diffraction data for compounds in Table 2, and IR spectra for **19** and **19**·AgOTf (PDF). This material is available free of charge via the Internet at http://pubs.acs.org.

JA991100B

(82) Kresge, C. T.; Leonowicz, M. E.; Roth, W. J.; Vartuli, J. C.; Beck, J. S. *Nature* **1992**, *359*, 710.